VIII International Conference on Computational Methods for Coupled Problems in Science and Engineering
COUPLED PROBLEMS 2019
E. Oñate, M. Papadrakakis and B. Schrefler (Eds)

A STATE-SPACE PARTITIONED TIME INTEGRATION ALGORITHM FOR REAL-TIME HYBRID SIMULATION WITH NONLINEAR NUMERICAL SUBDOMAINS

G. ABBIATI[1], I. LANESE[2], A. PAVESE[3], O.S. BURSI[4]

[1]Department of Engineering, University of Aarhus
Inge Lehmmans Gade, 10, 8000, Aarhus, Denmark
e-mail: abbiati@eng.au.dk

[2]EUCENTRE - European Centre for Training & Research in Earthquake Engineering
Via Ferrata 1, 27100 Pavia (PV), Italy
e-mail: igor.lanese@eucentre.it

[3]Department of Civil Engineering and Architecture, University of Pavia
Via Ferrata 1, 27100 Pavia (PV), Italy
e-mail: a.pavese@unipv.it

[4]Department of Civil, Environmental and Mechanical Engineering, University of Trento
Via Mesiano 77, 38123, Trento, Italy
e-mail: oreste.bursi@unitn.it

Key words: Hybrid Simulation; Partitioned Time Integration; State-Space Model; Seismic Isolation.

Abstract. This paper describes a state-space partitioned algorithm for real-time hybrid simulation. The state-space modeling is proposed to represent nonlinear numerical substructures. The effectiveness of the proposed method is demonstrated for a virtual bridge case study equipped with seismic isolation devices.

1 INTRODUCTION

Hybrid simulation (HS) merges structural testing and numerical modelling into a unique dynamic simulation paradigm, which has been extensively used to investigate the seismic response of civil structures [1]. In detail, a time stepping analysis algorithm solves for the coupled equation of motion of a prototype structure made of numerical and physical subdomains (NS and PS, respectively), which are assembled in a finite element (FE) fashion. On the PS side, servo-controlled actuators equipped with load cells impose displacement trials to the tested component and measure corresponding restoring forces. The NS is typically instantiated in a structural analysis software. In order to minimize actuator control errors, when the PS restoring force is rate independent, pseudodynamic- (PSD-) HS is performed, which means that the wall-clock duration of HS scales up with respect to the duration of the virtual excitation and velocities scale down of the same amount. If not, real-time- (RT-) HS is

performed. In both cases, PS testing is conducted by reproducing boundary and loading conditions as experienced within the prototype structure when subjected to a realistic excitation. Data from experiments is intended support model validation and calibration for tested structural components.

Most of developments related to HS consist on adaptations of existing FE analysis codes to accommodate so-called experimental elements, which incorporate a digital interface to the testing equipment. However, complexity of FE software, which trades off between modularity and computational performance, struggles with the deterministic execution scheduling imposed by RT-HS (i.e., evaluation of the NS response with a constant sampling period of 1÷10 msec). In our opinion, the state-space approach, which is quite popular in the control community, offers a computationally cheaper alternative to FE for modelling nonlinear NS. This paper describes a state-space partitioned time integration algorithm for RT-HS. The dual-coupling strategy of the modified-PH method [2] allows for assembling state-space equations of PS and NS in a FE fashion. HSs of a virtual two-pier reinforced concrete bridge equipped with friction pendulum bearings are presented as proof-of-concept example.

1 STATE-SPACE PARTITIONED ALGORITHM FOR HYBRID SIMULATION

In order to facilitate the assembly of nonlinear NSs simulated with well-known differential models (e.g. Mostaghel [3] hysteretic springs), the HS framework presented in this section relies on a newly conceived parallel partitioned algorithm tailored to state-space systems. The Monolithic-Generalized-α (MG-α) time stepping scheme proposed by Brüls and Arnold [4] is used as basic solver for the Partitioned-Generalized-α (PG-α) method, which adopts the coupling scheme of the modified PH method conceived by Brun and co-workers [2]. Both algorithms solve the system of equations of motion re-casted in state-space form that, for a generic nonlinear mechanical system, reads,

$$\mathbf{M}\dot{\mathbf{Y}} + \mathbf{R}(\mathbf{Y}) = \mathbf{F}(t) \tag{1}$$

where,

$$\mathbf{Y} = \begin{bmatrix} \mathbf{u} \\ \mathbf{v} \\ \mathbf{s} \end{bmatrix}, \mathbf{M} = \begin{bmatrix} \mathbf{I} & \mathbf{0} & \mathbf{0} \\ \mathbf{0} & \mathbf{m} & \mathbf{0} \\ \mathbf{0} & \mathbf{0} & \mathbf{I} \end{bmatrix}, \mathbf{R} = \begin{bmatrix} -\mathbf{v} \\ \mathbf{r}(\mathbf{u},\mathbf{v},\mathbf{s}) \\ \mathbf{g}(\mathbf{u},\mathbf{v},\mathbf{s}) \end{bmatrix}, \mathbf{F}(t) = \begin{bmatrix} \mathbf{0} \\ \mathbf{f}(t) \\ \mathbf{0} \end{bmatrix} \tag{2}$$

In detail, $\mathbf{u}, \mathbf{v}$ and $\mathbf{s}$ are displacement, velocity and additional state vectors, respectively. The former two always appear as a pair in second-order mechanical systems, while the latter is used to model nonlinearities endowed with memory (e.g., hysteresis). In particular, $\mathbf{r}(\mathbf{u},\mathbf{v},\mathbf{s})$ is the nonlinear restoring force vector while the nonlinear function $\mathbf{g}(\mathbf{u},\mathbf{v},\mathbf{s})$ comprises the evolution of the additional state vector $\mathbf{s}$. Moreover, $\mathbf{m}$ is the mass matrix and $\mathbf{f}(t)$ is the external time varying load while $\mathbf{I}$ and $\mathbf{0}$ are identity and zero matrices, respectively. When the system is linear, velocities and displacements only characterize the system state, which does not include additional variables. As a result, the restoring force reduces to,

$$\mathbf{r}(\mathbf{u},\mathbf{v}) = \mathbf{k}\mathbf{u} + \mathbf{c}\mathbf{v} \tag{3}$$

with $\mathbf{k}$ and $\mathbf{c}$ stiffness and damping matrices, respectively. For simplicity time dependency is omitted and hereinafter, $\mathbf{M}$, $\mathbf{K}$, $\mathbf{R}$ and $\mathbf{F}$ are referred to as generalized mass, stiffness, restoring force and external loading. First, the MG-α is presented; successively, the PG-α is described for coupling one PS and one NS.

1.1 The Monolithic G-α time integration algorithm

The original MG-α algorithm proposed by Jansen and co-workers [5] applied to integrate (1) from t_n to t_{n+1} with a time integration step $\Delta t = t_{n+1} - t_n$, reads,

$$\mathbf{M}\dot{\mathbf{Y}}_{n+\alpha_m} + \mathbf{R}\left(\mathbf{Y}_{n+\alpha_f}\right) = \mathbf{F}_{n+\alpha_f} \tag{4}$$

where,

$$\begin{aligned} \dot{\mathbf{Y}}_{n+\alpha_m} &= (1-\alpha_m)\dot{\mathbf{Y}}_n + \alpha_m \dot{\mathbf{Y}}_{n+1} \\ \mathbf{Y}_{n+\alpha_f} &= \left(1-\alpha_f\right)\mathbf{Y}_n + \alpha_f \mathbf{Y}_{n+1} \\ \mathbf{Y}_{n+1} &= \mathbf{Y}_n + \dot{\mathbf{Y}}_n(1-\gamma)\Delta t + \dot{\mathbf{Y}}_{n+1}\gamma\Delta t \end{aligned} \tag{5}$$

Parameters α_f, α_m and γ define the setting of the algorithm. They are expressed as function of the infinity spectral radius ϱ_∞ parameter as,

$$\alpha_m = \frac{3-\rho_\infty}{2(1+\rho_\infty)}, \alpha_f = \frac{1}{1+\rho_\infty}, \gamma = \frac{1}{2} + \alpha_m - \alpha_f \tag{6}$$

The resulting algorithm is second order accurate. In detail, if ϱ_∞ is chosen to be zero, the method annihilates the components of the system response whose frequencies are high compared to the sampling frequency. If $\varrho_\infty = 1$, then, $\alpha_m = \alpha_f = \gamma = 1/2$ and the MG-α method is equivalent to the trapezoidal rule, which does not introduce algorithmic dissipation.

1.2 The Partitioned G-α time integration algorithm

The PG-α method is a parallel partitioned time integration algorithm that couples two monolithic time integration processes based on the MG-α algorithm following a dual assembly approach. In detail, two parallel time integration processes are coupled at the coarse time step, where the compatibility of NS and PS is forced by a dual assembly procedure. The corresponding coupled system of equations of motion reads,

$$\begin{cases} \mathbf{M}^N\dot{\mathbf{Y}}^N_{n+1} + \mathbf{R}^N(\mathbf{Y}^N_{n+1}) = \mathbf{L}^N\boldsymbol{\Lambda}_{n+1} + \mathbf{F}^N_{n+1} \\ \mathbf{M}^P\dot{\mathbf{Y}}^P_{n+\frac{j}{ss}} + \mathbf{R}^P\left(\mathbf{Y}^P_{n+\frac{j}{ss}}\right) = \mathbf{L}^P\boldsymbol{\Lambda}_{n+\frac{j}{ss}} + \mathbf{F}^P_{n+\frac{j}{ss}} \\ \mathbf{G}^N\dot{\mathbf{Y}}^N_{n+1} + \mathbf{G}^P\dot{\mathbf{Y}}^P_{n+1} = \mathbf{0} \end{cases} \tag{7}$$

where, $\mathbf{M}, \mathbf{R}$ and $\mathbf{F}$ are defined in Eq. (2) while signed Boolean collocation matrices $\mathbf{L}$ and $\mathbf{G}$ localize interface forces and define compatibility equations, respectively. In line with Eq. (7), time steps Δt^N and Δt^P refer to simulation time, which is a virtual time axis defined by the time integration process. As an example, the seismic ground motion is expressed as function of the simulation time. In particular, Δt^N is the coarse time step adopted for the NS while Δt^P is the fine time step used to calculate the PS response. In order to guarantee a sufficient accuracy, $\Delta t^N = 1\ msec$ is typically considered. The testing time scale λ defines the ratio between wall-clock and simulation time speeds. In particular, when $\lambda = 1$ the test is conducted in real-time. Conversely, when $\lambda > 1$, the simulation time is extended in comparison with the wall-clock time and the test is conducted in a pseudodynamic regime. When the response of the PS does not depend on the rate of loading, λ usually ranges between 50 and 200. This approach reduces control tracking errors. Moreover, an extended simulation time scale λ reduces the destabilizing effect of actuator delay, which is typically of the order of $10 \div 20\ ms$. On the other hand, $\Delta t^S = \lambda \Delta t^N$ and $\Delta t^C = \lambda \Delta t^P$ refer to the wall-clock time, which is the real time flow measured in the laboratory. In particular, Δt^S defines the maximum solving time that can be allocated to compute the NS response while Δt^C is the actuator controller time step, which typically ranges between 1 and $2\ msec$ to guarantee smooth displacement trajectories. In principle, at each simulation step displacement and velocity solutions of Eq. (7) split into *free* and *link* components. The former are calculated discarding coupling conditions, which are used to compute the latter by means of a linearized Steklov-Poincaré operator. The coupled solution is the sum of both *free* and *link* contributions. Both free and link solutions are solved based on the MG-α algorithm, which provides tunable algorithmic damping to the coupled scheme.

2 THE VIRTUAL TWO-PIER BRIDGE

2.1 Description of the case study

In order to verify the proposed computational framework, we conceived a two-pier bridge case study that we used to benchmark three alternative seismic isolation schemes. The virtual bridge prototype depicted in Figure 1 is characterized by a three-span reinforced concrete deck with two independent roadways, sustained by two twin cantilever rectangular hollow cross-section RC piers. Cross sections of deck and pier are depicted in Figure 2. As depicted in Figure 1, a pair of seismic isolation devices was interposed between deck and piers and deck and abutments.

Three alternative seismic isolation devices were tested, namely, double and triple concave sliding bearing (D- and T-CSB, respectively) and lead rubber bearing (LBR). All devices were dimensioned to keep the maximum transversal shear force applied to each pier below $370\ kN$ and the corresponded transversal displacement below $3\ mm$.

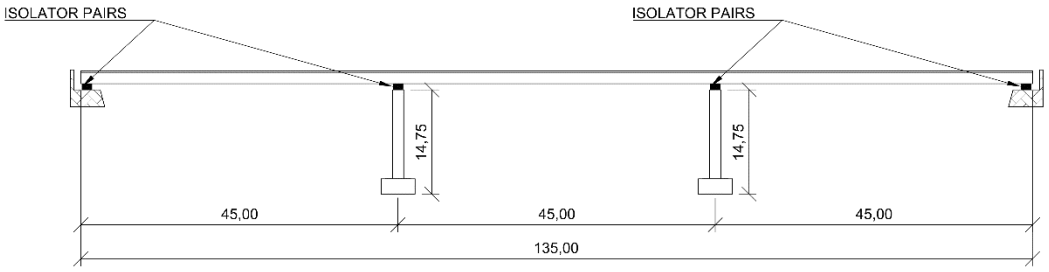

Figure 1: Virtual bridge prototype.

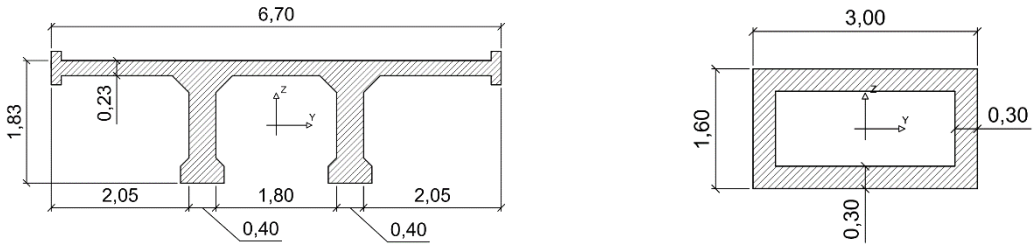

Figure 2: Cross-sections of: a) deck; b) pier.

Due to the limited length of the paper, only the T-CSB device is described. Figure 3 depicts a schematic of a generic T-CSB device, for which a detailed mechanical model can be found in [6].

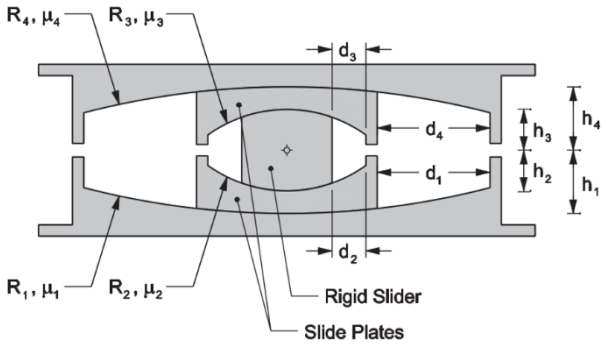

Figure 3: Schematic of a T-CSB device after [6].

The REXEL software [7] was used to select a single ground motion record corresponding to a seismic scenario characterized by moment magnitude $M = 5 \div 7$, epicentral distance $D = 0 \div 30$ km and soil type B, which was scaled to different values of peak ground acceleration (PGA). In detail a PGA value of 0.12 g was assigned to the serviceability limit state (SLS) while a PGA value of 0.30 g was selected for the ultimate limit state (ULS) based on a comprehensive analysis of the bridge response based on a nonlinear FE model. The horizontal seismic excitation was orthogonal to the main axis of the bridge deck.

2.2 Substructuring scheme

Figure 4 depicts the partitioning of the virtual bridge prototype into PSs and NSs, which are colored in red and blue, respectively. In detail, nonlinear springs represent piers and seismic isolation device pairs, while the continuous line is the deck. The latter was obtained via static condensation of a linear FE model based on Bernoulli beam elements, by retaining transversal displacements of Nodes #1, #6, #11 and #16, that is, connection points to piers and abutments.

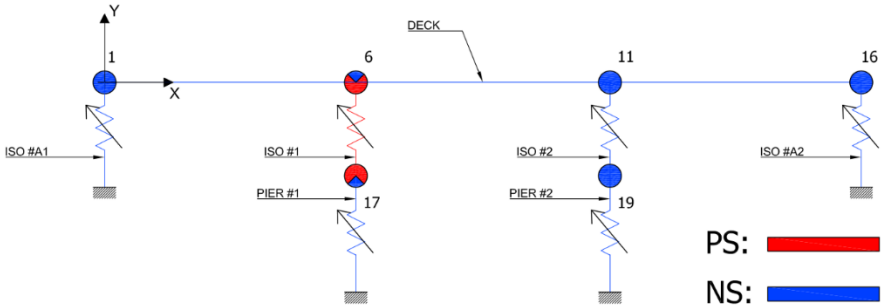

Figure 4: Plan views of the substructured virtual bridge prototype.

As can be appreciated from Figure 4, one pair of T-CSB devices was tested in the laboratory while all other substructures were simulated numerically. In order to reproduce the hysteretic response of the T-CSB on the NS, a state-space model inspired to Mostaghel's work [3] was developed. In this regard, Figure 5 shows both the spring-slider idealization and the entailing hysteretic loop.

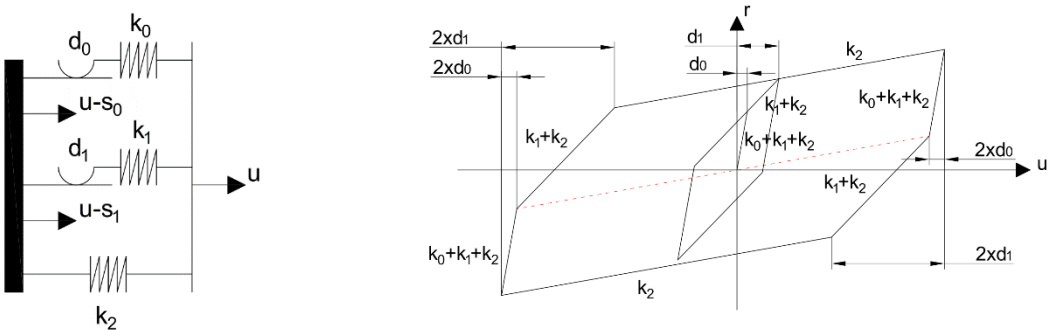

a b

Figure 5: T-CSB state-space model: a) spring-slider idealization; b) hysteretic loops.

The state-space model of the restoring force r is described as,

$$\begin{aligned} \dot{r} &= \dot{r}_0 + \dot{r}_1 + \dot{r}_2 \\ \dot{r}_0 &= \left(k_0\left(\bar{N}(v)\bar{M}(s_0 - \delta_0) + M(v)N(s_0 + \delta_0)\right)\right)v \\ \dot{r}_1 &= \left(k_1\left(\bar{N}(v)\bar{M}(s_1 - \delta_1) + M(v)N(s_1 + \delta_1)\right)\right)v \\ \dot{r}_2 &= k_2 v \end{aligned} \tag{8}$$

where slip displacements of equivalent sliders read,

$$\begin{aligned} s_1 &= r_1/k_1 \\ s_2 &= r_2/k_2 \end{aligned} \tag{9}$$

and functions $N, M, \bar{N}$ and $\bar{M}$ read,

$$\begin{aligned} N(w) &= 0.5\big(1 + sgn(w)\big)\Big(1 + \big(1 - sgn(w)\big)\Big) \\ M(w) &= 1 - N(w) \\ \bar{N}(w) &= M(-w) \\ \bar{M}(w) &+ N(-w) \end{aligned} \tag{10}$$

Values of model parameters identified for the maximum velocity peak of 0.1 m/s read,

$$k_0 = 6.67e7\ N/m\,, \delta_0 = 1.5e-3m,\ k_1 = 1.15e6\ N/m\,, \delta_1 = 0.07m,\ k_2 = 5e5\ N/m$$

The developed model was validated against experimental data. In this respect, Figure 6 compares emulated and measured hysteretic loops and dissipated energy histories. As can be appreciated, the developed model accurately reproduces the response of the tested T-CSB device.

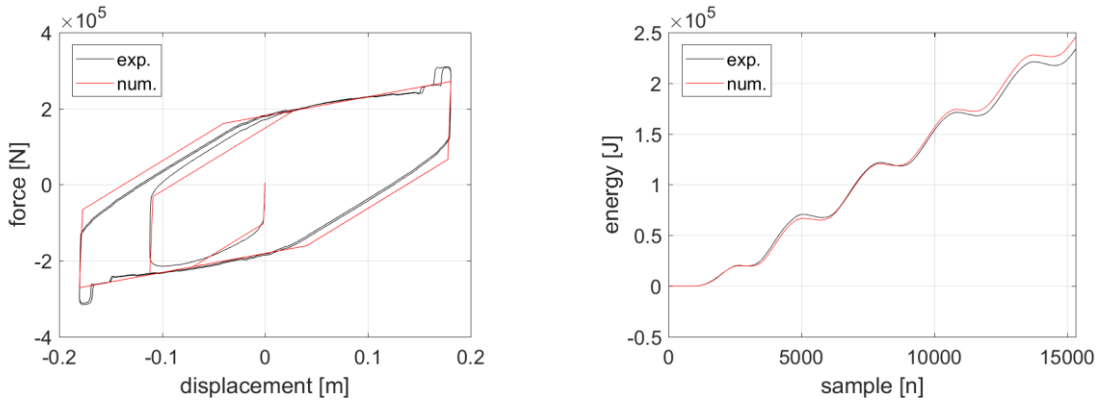

a b

Figure 6: Validation of the D-CSB model against experimental measurements at $v = 0.1$ m/s: a) hysteretic loop; b) dissipated energy.

3 HYBRID SIMULATION OF THE VIRTUAL BRIDGE

3.1 Architecture of the implementation

In order to simulate the virtual bridge prototype, the HS framework of Figure 7, which relies on the PG-α algorithm described in Section 1, was implemented at the Experimental Laboratory of EUCENTRE, Pavia, Italy. A Windows-based HOST-PC runs the MATLAB-SIMULINK

computational environment [8], which implements both the PG-α algorithm and the NS of the substructured system. The C-code automatically generated by SIMULINK is compiled and uploaded to the XPC-TARGET that executes the software in real-time. The XPC-TARGET is provided with DAQ boards that communicate with the Bearing Testing System (BTS) controller, which controls a servo-hydraulic loading system specifically conceived for testing bearings. At each simulation step of the PG-α algorithm, the XPC-TARGET sends displacement commands to the physical D-CSB, and the related restoring force is fed back to the PG-α algorithm that solves the system of coupled equations of motion. In order to enable fast-time testing i.e., $\lambda = 2 \div 20$, the delay compensation algorithm proposed by Wu and co-workers [9], was adopted.

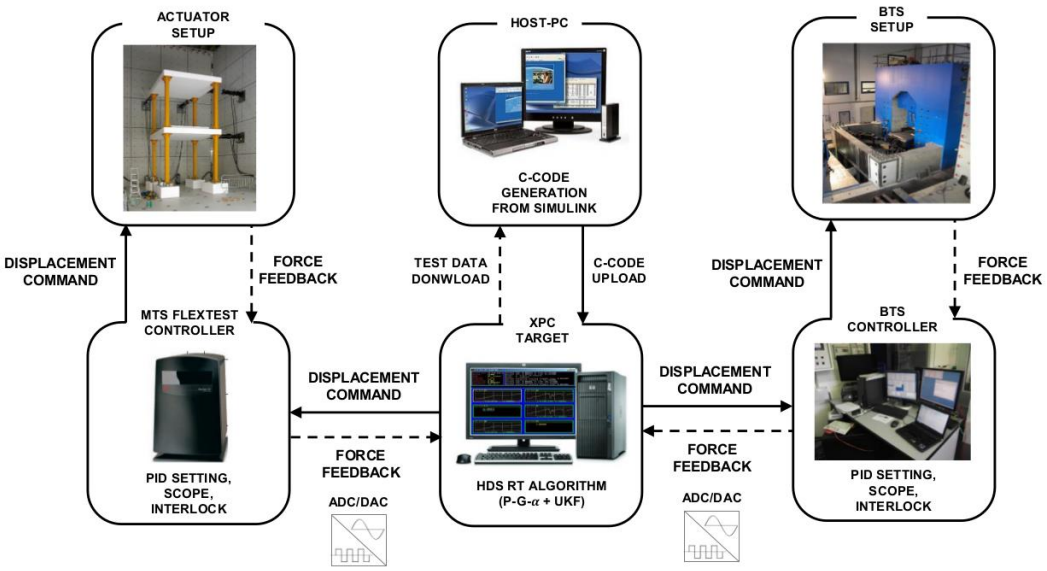

Figure 7: Block diagram of the HS framework.

The BTS of the Experimental Laboratory of EUCENTRE has been specifically designed to impose realistic boundary conditions to full-scale seismic isolation devices [10]. In this regard, Figure 8 shows the BTS setup and provides a close-up view of the restoring force measuring system. In detail, the specimen is positioned on a self-equilibrating vertical reaction structure; the bottom plate of the specimen is connected to a 6-DoF shake table, driven by vertical and horizontal actuators and connected to an additional horizontal reaction structure, which can be operated in mixed force-displacement control. The maximum vertical and horizontal load capacities of the BTS are $50\,MN$ and $2.8\,MN$, respectively. The allowed horizontal displacement range is $\pm\,495\,mm$ with a velocity peak of $2200\,mm/s$. During standard characterization tests, the load cells of the horizontal actuators measure the raw restoring force of the specimen, which is post-processed offline to remove machine inertia and friction. In order to skip this task during HS, a force measuring system is developed. It is based on a steel plate sliding on a Teflon layer and surrounded by 8 ring pre-stressed load cells, which measure the specimen restoring force in two orthogonal plane directions.

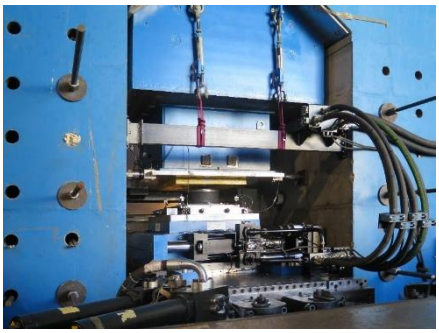

Figure 8: Bearing Testing System (BTS).

Since energy dissipation in seismic isolation devices mainly relies on friction or damage mechanisms, they are easily biased when devices are scaled. Accordingly, full-scale devices are considered in this testing campaign. It is worthy to note that the interaction between displacement controlled actuators and stiff specimens easily triggers dynamic instability. This situation is very likely to occur on elements subjected to axial deformation, where small displacement perturbations generate large feedback forces. In order to overcome this problem, the common practice consists on excluding vertical degrees-of-freedom from the HS loop and impose nominal loads in force control. Accordingly, the nominal vertical load owing to the self-weight of the bridge deck is kept constant and applied to the tested seismic isolation device in force control. In addition, a single bearing per pair is physically tested and the measured restoring force feedback to the HS algorithm is doubled. This latter simplification was preliminary verified with numerical simulations, which prove that deck overturning moment is negligible and does not affect the transversal response of the bridge.

3.2 **Results of experiments**

The HS campaign started on February 2015 and ended in April 2017. Experiments were conducted by scaling the reference ground motion record up to a PGA value of 0.85 g. Figure 9 compares the hysteretic loops of the restoring forces of tested isolation devices, which show similar forces and displacement ranges. This trend confirms that the investigated isolation schemes highlight similar performances.

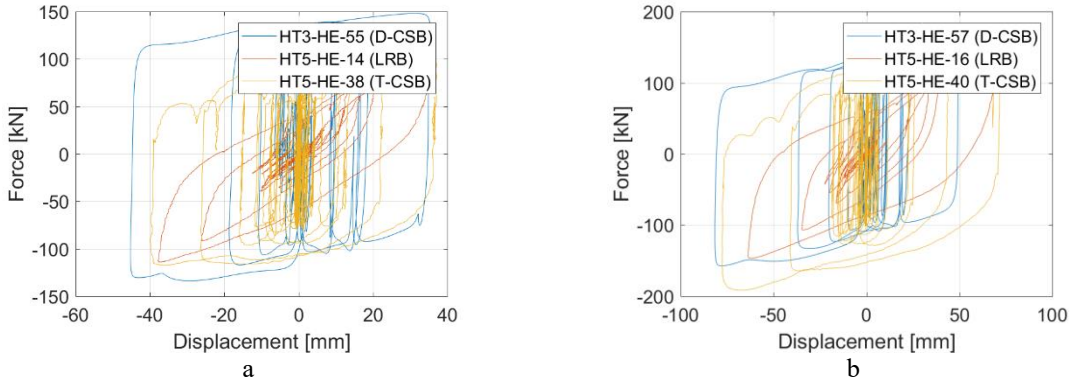

a b

Figure 9: Hysteretic loops of different isolator devices at: a) PGA = 0.35g; b) PGA=0.50g.

4 CONCLUSIONS

This paper presented a state-space partitioned time integration algorithm for real-time hybrid simulation. State-space modeling simplifies the implementation of nonlinearities on the numerical substructures, which can be incorporated with a lower computational cost compared to the finite-element modeling paradigm. The effectiveness of the proposed method is demonstrated for a virtual two-pier bridge case study equipped with friction pendulum bearings.

5 ACKNOWLEDGMENTS

The authors wish to acknowledge Dr. Enrico Cazzador for having dimensioned the virtual bridge case study as part of his doctoral thesis and the laboratory technicians of the European Centre for Training & Research in Earthquake Engineering, Pavia, Italy.

6 REFERENCES

[1] A. H. Schellenberg, S. A. Mahin e G. L. Fenves, «PEER Report 2009/104 "Advanced Implementation of Hybrid Simuation",» Pacific Earthquake Engineering Research (PEER) Center, University of California, Berkeley, 2009.

[2] M. Brun, A. Batti, A. Combescure e A. Gravouil, «External coupling software based on macro- and micro-time scales for explicit/implicit multi-time-step co-computations in structural dynamics,» *Finite Elements in Analysis and Design,* vol. 86, p. 101–119, 2014.

[3] N. Mostaghel, «Analytical Description of Pinching, Degrading Hysteretic Systems,» *Journal of Engineering Mechanics,* vol. 2, n. 216–224, p. 125, 1999.

[4] O. Brüls e M. Arnold, «The Generalized-α Scheme as a Linear Multistep Integrator: Toward a General Mechatronic Simulator,» *Journal of Computational and Nonlinear Dynamics,* vol. 3, n. 4, p. 41007, 2008.

[5] K. E. Jansen, C. H. Whiting e G. M. Hulbert, «A generalized-α method for integrating the filtered Navier–Stokes equations with a stabilized finite element method,» *Computer Methods in Applied Mechanics and Engineering,* vol. 190, n. 3-4, p. 305–319, 2000.

[6] D. M. Fenz e M. C. Constantinou, «Spherical sliding isolation bearings with adaptive behavior: theory,» *Earthquake Engineering & Structural Dynamics,* vol. 37, n. 2, p. 163–183, 2008.

[7] I. Iervolino, C. Galasso e E. Cosenza, «REXEL: computer aided record selection for code-based seismic structural analysis,» *Bulletin of Earthquake Engineering,* vol. 8, n. 2, pp. 339-362, 2010.

[8] MathWorks, «MATLAB webpage,» MathWorks, 7 2 2018. [Online]. Available: https://ch.mathworks.com/. [Consultato il giorno 7 2 2018].

[9] B. Wu, Z. Wang e O. S. Bursi, «Actuator dynamics compensation based on upper bound delay for real-time hybrid simulation,» *Earthquake Engineering & Structural Dynamics,* vol. 42, n. 12, p. 1749–1765, 2013.

[10] S. Peloso, A. Pavese e C. Casarotti, «Eucentre TREES Lab: Laboratory for Training and Research in Earthquake Engineering and Seismology,» in *Role of Seismic Testing Facilities in Performance-Based Earthquake Engineering*, Dordrecht, Springer Netherlands, 2012, pp. 65--81.